

See discussions, stats, and author profiles for this publication at: <https://www.researchgate.net/publication/51039514>

Two-Phase Synthesis of Monodisperse Silica Nanospheres with Amines or Ammonia Catalyst and Their Controlled Self-Assembly

ARTICLE in ACS APPLIED MATERIALS & INTERFACES · MAY 2011

Impact Factor: 6.72 · DOI: 10.1021/am200104m · Source: PubMed

CITATIONS

35

READS

228

6 AUTHORS, INCLUDING:



Junzheng Wang

The University of Tokyo

13 PUBLICATIONS 99 CITATIONS

SEE PROFILE



Ayae Sugawara-Narutaki

Nagoya University

30 PUBLICATIONS 176 CITATIONS

SEE PROFILE



Toshiyuki Yokoi

Tokyo Institute of Technology

128 PUBLICATIONS 3,468 CITATIONS

SEE PROFILE



Atsushi Shimojima

Waseda University

106 PUBLICATIONS 2,068 CITATIONS


SEE PROFILE

Two-Phase Synthesis of Monodisperse Silica Nanospheres with Amines or Ammonia Catalyst and Their Controlled Self-Assembly

Junzheng Wang,[†] Ayae Sugawara-Narutaki,[†] Masashi Fukao,[†] Toshiyuki Yokoi,[‡] Atsushi Shimojima,[†] and Tatsuya Okubo^{*,†}

[†]Department of Chemical System Engineering, The University of Tokyo, 7-3-1 Hongo, Bunkyo-ku, Tokyo 113-8656, Japan

[‡]Chemical Resources Laboratory, Tokyo Institute of Technology, 4259 Nagatsuta, Midori-ku, Yokohama 226-8503, Japan

 Supporting Information

ABSTRACT: A significant progress has recently been made in the synthesis of monodisperse silica nanoparticles less than 30 nm in diameter by using basic amino acids (e.g., lysine) as a base catalyst for hydrolysis of silicon alkoxide. Alternatively, a more versatile and economical amino acid-free method has been developed to synthesize uniform silica nanospheres (SNSs) with low polydispersity (<12%) in liquid–liquid biphasic systems containing tetraethoxysilane (TEOS), water, and primary amine (or ammonia) under precisely controlled pH conditions (pH 10.8–11.4). The diameter of the SNSs determined from scanning electron microscopy (SEM) can be tuned from ~12 to ~36 nm by simply changing the initial pH of the aqueous phase in the reaction mixtures. Furthermore, the as-synthesized sol was taken as the starting material for studying the influences of the type of base catalysts on the solvent evaporation-induced three-dimensional (3D) self-assembly of SNSs. X-ray diffraction (XRD) and nitrogen adsorption–desorption are used to characterize the degree of packing of the resulting 3D arrays. The assembled SNSs with large interparticle mesopores with the diameter of ca. 8.1 nm and low packing fraction of ca. 66.1% are observed upon solvent evaporation of as-synthesized sol in the presence of primary amine. This indicates that SNSs are loosely packed, compared with the packing fraction of 74% for a face-centered cubic array of ideal hard spheres. In contrast, with the aid of an organic buffer or lysine as additives, the assembly of SNSs having smaller mesopores (ca. 3.9 nm) and higher packing fraction of 70.5–71.5% are achieved. It is suggested that the chemical additives with the ability to maintain relatively strong repulsive interaction until the final stage of evaporation play a vital role in the fabrication of well-ordered SNSs arrays.

KEYWORDS: colloid, silica nanospheres, self-assembly

1. INTRODUCTION

Monodisperse colloidal particles have attracted much attention not only for their fundamental scientific interest but also for many technological applications.^{1–4} Among various colloidal particles, silica particles occupy one of the most important positions in the fields of materials and colloid science because of the ease of their preparation and functionalization, as well as a wide range of applications.^{5–7} Colloidal silica particles are also useful as hard templates for the synthesis of other functional materials.^{8–14} Inorganic and hybrid hollow capsules have been obtained by utilizing silica particles as sacrificial templates.^{8–10} Ordered colloidal crystals, which are formed through the self-assembly of monodisperse silica particles, are frequently used for the fabrication of various porous materials.^{11–14} In most cases, the synthesis of colloidal silica particles with uniform and tunable sizes is essential.

The Stöber method has been widely used for the preparation of monodisperse colloidal silica particles.¹⁵ They are produced through hydrolysis and polycondensation of silicon alkoxides (e.g., tetraethoxysilane (TEOS)) in the single-phase system in the presence of ammonia as a catalyst and alcohol–water media. However, synthesis of small silica nanoparticles with diameter less than 30 nm and low polydispersity (<20%) is still challenging for the Stöber method.¹⁶ An alternative, widely used strategy for synthesis of small silica nanoparticles with diameter below 50 nm and low polydispersity (<15%) is water–in–oil reverse microemulsion-mediated synthesis.^{17–24} Microemulsion acts as a

versatile microreactor for the confined synthesis of silica nanoparticles. However, due to the uses of large amounts of organic solvents and surfactants, microemulsion method possesses distinct disadvantages in costs, purification, and nanoparticles recovery for the large-scale synthesis.

We have recently made an important breakthrough in synthesizing uniform-sized silica nanospheres (SNSs) with diameter ranging from 12 to 44 nm.^{25,26} The SNSs are synthesized by hydrolysis and polycondensation of TEOS in the two-phase system in the presence of basic amino acid (lysine) and water without using any surfactants or organic cosolvents. The reaction system has the following features: (i) immiscible liquid–liquid (TEOS–water) biphasic system, (ii) weakly basic, and (iii) almost constant pH condition (pH 9–10). The latter two features are due to the relatively weak basicity and the buffering capability of the basic amino acid. Under such a condition, silicate species are slowly supplied to the water phase because of the limited contact areas between TEOS and water phases in addition to slow hydrolysis rate of TEOS at moderate pH. Silicate species thus provided are immediately consumed for the growth of primary particles (nuclei) because of the exceedingly low solubility of the silicates and relatively high condensation

Received: January 26, 2011

Accepted: April 11, 2011

Published: April 11, 2011

rate at pH 9–10. Tsapatsis and co-workers also reported the formation of small sized silica nanoparticles (~ 5 nm) in the presence of a considerable amount of lysine.²⁷ Hartlen et al. synthesized monodisperse silica particles with the size ranging from 15 to 200 nm by using seed regrowth method based on our approach.²⁸ Most recently, Watanabe et al. prepared silica particles with sizes up to 550 nm through the seed regrowth method, where ethanol–water mixed medium containing arginine was used.²⁹ Furthermore, mesoporous silica nanospheres were prepared by adding surfactants in TEOS–water biphasic system in the presence of arginine as a catalyst.³⁰

Another important finding is that such SNSs can assemble into three-dimensional (3D), well-ordered close packed structure (face-centered-cubic) upon solvent evaporation.^{25,26,31,32} It was supposed that the constant pH condition (~ 9) until the final stage of solvent evaporation owing to the buffering capability of basic amino acids might be the key to the formation of highly ordered structures.²⁶ In such a condition, SNSs are electrostatically repulsive (zeta potential ca. -40 mV) until the very last moment of solvent evaporation, which prevents SNSs from random aggregation. Interestingly, we also found out that such SNSs assemble into 1D chainlike nanostructure in a liquid phase with the aid of an amphiphilic block copolymer F127.³³

As described above, preparation of SNSs with basic amino acids in the TEOS–water biphasic system and the ordered assembly of SNSs from the corresponding sols have attracted much attention.^{26–29,31–33} However, it has been still unclear whether the use of amino acid as a catalyst is indispensable or not for the synthesis of monodisperse SNSs and their ordered assembly. One of the next important steps to be explored is the synthesis of SNSs without using amino acid but with more common basic catalysts such as primary amines and ammonia. These amino acid-free SNSs will help us to understand the role of base catalysts for the synthesis and assembly of SNSs more clearly through the comparative experiments. Moreover, such SNSs have significant advantages in the practical use: low cost and easy removal of the catalysts from SNSs due to their relatively low boiling points. In the previous report, we tried to prepare SNSs in a TEOS–water biphasic reaction system by using ammonia instead of lysine at the same molar ratio;²⁶ however, a preliminary experiment resulted in the formation of irregularly assembled silica nanoparticles through evaporation of the corresponding sol. The discussion about the monodispersity of the nanoparticles was difficult because of the highly aggregated structure.

Here we report the synthesis of monodisperse colloidal SNSs in TEOS–water biphasic system by using primary amines or ammonia without buffering capability. A thorough investigation of the effect of pH (the amount of catalysts) has revealed that monodisperse SNSs are successfully synthesized with these base catalysts under relatively high pH conditions. The final size of SNSs is systematically tuned by simply changing the initial pH of the water phase. The most important finding here is that monodisperse SNSs can be obtained under unbuffered conditions where pH of the reaction system decreases after the reaction. The amino acid-free SNS sols thus obtained are used for the study of solvent evaporation-induced 3D self-assembly of SNSs. The degree of long-range ordering of the assembled SNSs has been examined by X-ray diffraction (XRD) and nitrogen adsorption–desorption. Loosely packed SNSs arrays are formed via solvent evaporation of the as-synthesized SNSs sols. The addition of organic molecules having buffering capability enhances the degree of SNSs packing regularity. These results

suggest that the textural properties (total pore volumes and pores sizes) of the 3D assembled SNSs can be easily tailored by adjusting the composition of SNSs sols.

2. EXPERIMENTAL SECTION

2.1. Materials. TEOS was obtained from Tokyo Chemical Industry Co., Ltd. and used without further purification. *N*-Cyclohexyl-2-aminoethanesulfonic acid (CHES) ($pK_a = 9.3$), sodium hydroxide (50 wt % NaOH in water), *n*-butylamine, *n*-propylamine, 25 wt % ammonia solution, and L-lysine were purchased from Wako Pure Chemical Industries Ltd. and used as received. Silicon wafers (SEH, Inc.) were treated with Semico Clean 56 (Furuuchi Chemical) and washed with deionized water in an ultrasonic bath for 20 min. The wafers were then rinsed thoroughly in ethanol, followed by air drying at room temperature. Milli-Q water (18.2 M Ω cm^{-1}) was used for all the experiments.

2.2. Preparation of Catalyst Stock Solutions. Catalyst stock solutions were prepared as follows; each base catalyst (25 wt % ammonia solution, *n*-propylamine, and *n*-butylamine) was added dropwise to water (500 g) at room temperature to make the stock solution with pH ranging from 9.2 to 11.4. They were stored in a tightly sealed bottle to maintain their pH for a long time.

2.3. Synthesis of Uniform-Sized SNSs. In a typical synthesis, a catalyst stock solution (34.75 g) was transferred to a 110 mL glass vial. Subsequently, TEOS (2.60 g) was added to the catalyst solution at one time and then the resultant TEOS–water biphasic system was stirred at 60 °C for 24 h in a water bath. The magnetic stirring rate was kept at ca. 500 rpm using a 2 cm long Teflon-coated stirring bar. A homogeneous, optically clear colloidal suspension of SNSs was obtained finally.

2.4. Solvent Evaporation Induced 3D Self-Assembly Process. The SNSs were assembled in the presence or absence of chemical additives by solvent evaporation-induced self-assembly process. Lysine and CHES were used as additives, and each of them was added into the as-synthesized SNSs sols to the final concentration of 7 mM (pH 9.5) and 10 mM (pH ~ 6), respectively. The pH of SNSs sol containing CHES was then adjusted to 9.5 with a 50 wt % sodium hydroxide solution. The SNSs sols (35 mL) with or without additives were added into 110 mL glass vials. They were dried at 60 °C under normal atmospheric conditions for 24 h, yielding translucent solids.

2.5. Characterization. Scanning electron microscope (SEM) images were taken on Hitachi S-900 with an accelerating voltage of 6 kV. Samples were dip-coated on Si wafers. To minimize sample charging, the samples were coated with Pt just before SEM observation in an argon atmosphere using an ion sputter system, Hitachi E-1030. The pH was measured using a HORIBA pH meter D-52. The pH meter was calibrated with standardized buffer solutions (pH 4.01, 6.86, and 9.18) before the measurement. Zeta potential measurements were performed with a Malvern Zetasizer Nano ZS90 instrument at 25 °C. The zeta potentials of SNSs were calculated from the electrophoretic mobility using the Helmholtz–Smoluchowski equation. Fourier transform infrared (FT-IR) spectra were obtained in the region of 400–4000 cm^{-1} on a Magna-IR 560 (Nicolet Instrument Corp.) by the KBr pellet technique (1 mg of sample in 100 mg of KBr). CHN elemental analyses were performed on CE-440 (Elemental Analysis, Inc.). Powder X-ray diffraction (XRD) patterns were recorded on a Bruker AXS M03X-HF diffractometer with Cu K α radiation at 40 kV and 30 mA in the 2θ range of 0.35–3.5°. Samples were calcined at 550 °C for 5 h and ground before the measurements. Nitrogen adsorption and desorption isotherms at 77 K were measured on Autosorb-1 (Quantachrome Instruments). After calcination at 550 °C for 5 h, samples were degassed at 250 °C for 10 h. The pore size distributions were derived from the adsorption branches of the isotherms based on the Barrett–Joyner–Halenda (BJH) model. The total pore volumes were estimated from the amount adsorbed at a relative pressure of about 0.99.

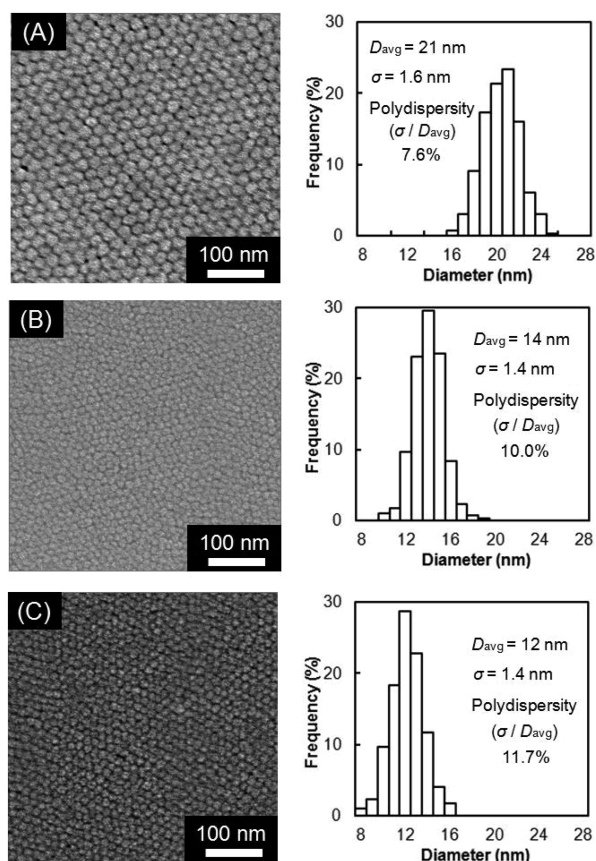


Figure 1. SEM images of SNSs catalyzed by *n*-butylamine at different pH conditions (left) and corresponding size histograms obtained by statistical analysis of over 300 SNSs (right): (A) pH 10.8, (B) pH 11.2, and (C) pH 11.4.

3. RESULTS AND DISCUSSION

3.1. Synthesis of Uniform-Sized SNSs with Tunable Sizes.

TEOS was hydrolyzed and condensed in liquid–liquid (TEOS–water) biphasic systems using primary amines (*n*-propylamine or *n*-butylamine) or ammonia as base catalysts. Figure S1 shows the pH of the aqueous solutions of base catalysts as a function of their concentrations. The pH of the solution increases with increasing the concentrations of base catalysts. The pK_a values of *n*-propylamine, *n*-butylamine, and ammonia are 10.6, 10.7, and 9.3 in water, respectively. *n*-Propylamine and *n*-butylamine are similar in base strength, whereas ammonia shows weaker basicity.

Syntheses of SNSs have been carried out at several different pHs by changing the concentration of base catalysts while the other reaction conditions remained unchanged. It has been revealed that the initial pH of the water phase has a major influence on the final size of SNSs. SEM images of SNSs formed in the presence of *n*-butylamine are shown in Figure 1. They were dip coated onto Si substrates from their colloidal system to give close-packed ordered arrangements. At pH 10.8 (Figure 1A), monodisperse SNSs with an average diameter of 21 nm and a size polydispersity of 7.6% are observed. Upon raising the pH to 11.2 (Figure 1B), SNSs with uniform size of about 14 nm and a polydispersity of 10% are found. At pH 11.4 (Figure 1C), SNSs with the smallest size of about 12 nm and the largest polydispersity of 11.7% are obtained. Above pH 11.5, it was hard to observe

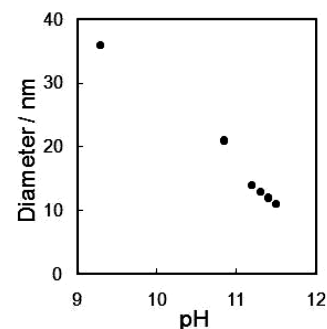


Figure 2. Relationship between the initial pH of the water phase and the average diameter of SNSs formed in the presence of *n*-butylamine.

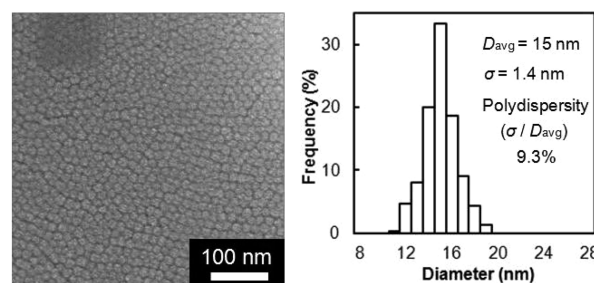


Figure 3. A SEM image of SNSs formed in the presence of ammonia (pH 10.8) (left) and the corresponding size histogram obtained by statistical analysis of over 300 SNSs (right).

nanoparticles, probably because of their smaller sizes below the resolution limit of the SEM. Nanoparticles with increased diameters (~ 36 nm) with rough surfaces are produced at lower pH conditions (pH 9.0–9.5) (see Figure S2 in the Supporting Information).

Figure 2 summarizes the relationships between the initial pH of the water phase and the average diameter of the resultant SNSs. This clearly shows that the final size of SNSs can be finely tuned by simply changing the initial pH of the reaction solution. Similarly, using *n*-propylamine as a base catalyst, the same trend of a steady decrease in SNSs size with increasing the pH has been confirmed (see Figure S3 in the Supporting Information). This tendency was also observed in the case of lysine-catalyzed system.²⁶ Ammonia also gives monodisperse SNSs in the TEOS–water biphasic reaction system. For example, SNSs with average diameter of 15 nm and a size polydispersity of 9.3% are obtained with ammonia (pH 10.8) (Figure 3). It should be noted that the concentration of ammonia used here is in the range of tenths of millimolar, which is much lower than that in the Stöber method (3–8 M).¹⁵

The details of the reaction have been investigated in the representative *n*-butylamine-catalyzed system. The disappearance of the oil phase (TEOS), which is an indication of near-complete hydrolysis of TEOS, is achieved within 1 day at relatively high initial pH (10.8–11.4), whereas it takes about 10 days at lower initial pH (9.0–9.5). The hydrolysis rate at lower pH is surprisingly slow compared to that in lysine-catalyzed reaction where hydrolysis is completed within 1 day even at initial pH of ~ 9.8 .^{25,26} It is known that the rate of base-catalyzed hydrolysis of TEOS increases with increasing pH. The difference in the hydrolysis rates between *n*-butylamine- and lysine-catalyzed reactions can be attributed to the difference in

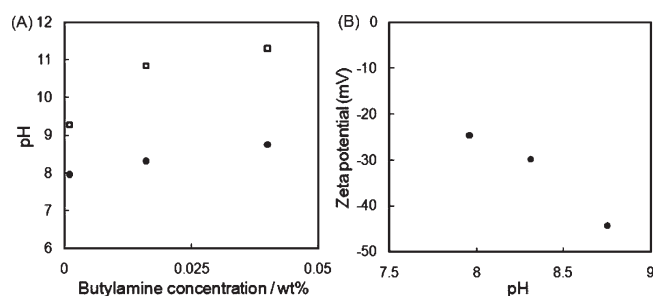
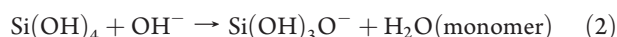
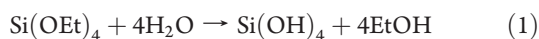


Figure 4. (A) Variation in pH as a function of *n*-butylamine concentration before and after reaction. Open square symbols (□) represent the initial pH before reaction; solid circle symbols (●) represent the final pH after complete disappearance of TEOS phase. (B) The zeta potential of SNSs synthesized with *n*-butylamine as a function of the final pH of sols.

the pH variations before and after reaction. A substantial decrease in pH takes place during the reaction in the presence of *n*-butylamine as shown in Figure 4A. For example, the pH decreases from 11.3, 10.8, and 9.3 to 8.8, 8.3, and 8.0, respectively, after complete disappearance of TEOS phase. This significant pH drop is possibly due to the following series of acid–base reactions



In contrast, when basic amino acid lysine was used as a catalyst for SNSs synthesis, only a slight reduction in pH from ~ 9.8 to ~ 9.2 was observed owing to its buffering capability.^{25,26} Although it had been anticipated that the constant pH condition during particle formation is advantageous for the formation of monodisperse SNSs, the results have revealed that uniform-sized SNSs can also be prepared under unbuffered conditions, where the hydrolysis rate of TEOS, condensation rate of silicate species, and the solubility of silicate species drastically change along with the decrease in pH. As similar as amino acid-catalyzed system,²⁶ hydrolysis of TEOS is quite slow in the present system, because this reaction occurs at the liquid–liquid (TEOS–water) interface. Namely, silicate species are of restrict supply due to the limited surface area of the TEOS–water interface. On the other hand, as the reaction proceeds, condensation process becomes faster, which is caused by the decrease of pH in water phase due to the amines or ammonia without buffering capability. These features are the key factors for two-phase synthesis of monodisperse SNSs with amines or ammonia catalyst.

As described above, monodisperse SNSs are obtained in the presence of *n*-butylamine at higher initial pH (10.8–11.4), whereas the bigger nanoparticles with rough surfaces are produced at lower pH (9.0–9.5). It appears that the individual bigger nanoparticles consist of several primary particles (see Figure S2 in the Supporting Information). This result can be explained by the low surface electric potential of silica nanoparticles. Figure 4B shows the zeta potentials of SNSs as a function of the final pH of the reaction media. SNSs are more negatively charged at higher pH. For example, the zeta potentials of SNSs are -24.6 and -44.4 mV at pH 8.0 and 8.8, respectively. SNSs are electrostatically repulsive and thus colloiddally stable throughout the reaction if the starting pH is sufficiently high. The low

initial pH (~ 9.3) in turn leads to the much lower final pH (~ 8.0), where the growing particles tend to aggregate because of the reduction of electrostatic repulsion.

3.2. 3D Self-Assembly of Monodisperse SNSs by Solvent Evaporation. As mentioned in the previous section, monodisperse SNSs are successfully synthesized by using primary amines or ammonia in the TEOS–water biphasic reaction system. The colloidal suspensions thus obtained can be used as good starting materials to study 3D self-assembly of SNSs. In the previous reports, we^{25,26} and Snyder et al.³² showed that SNSs sols prepared with lysine gave well-ordered, close-packed 3D structures by simply evaporating the solvent. We have proposed that the constant pH condition (pH ~ 9.4) during the solvent evaporation due to the buffering capability of basic amino acid is responsible for the regular assembly of SNSs, since such a condition prevents SNSs from random aggregation by keeping SNSs electrostatically repulsive (zeta potential ca. -40 mV) until the final stage of solvent evaporation. In addition, a considerable amount of amino acids are adsorbed on SNSs surface; therefore, hydrogen bond formation between amino acids at the end of solvent drying up might be involved in the formation of close-packed structure.^{26,31}

In contrast to the system containing basic amino acids, totally different situations would be expected in the case of SNSs sols prepared with primary amines or ammonia. Because of the low boiling points (48, 78, and -33 °C for *n*-propylamine, *n*-butylamine, and ammonia, respectively) of these simple catalysts, they will evaporate faster than water. The evaporation of the base catalysts from the system will cause the decrease in pH in the course of solvent evaporation, leading to the colloidal instability of SNSs. Indeed, we have observed experimentally that there are almost no catalysts remain on SNSs surfaces after solvent evaporation by FT-IR spectroscopy and elemental analysis (see Figures S4 and Table S1 in the Supporting Information). It has also been verified that the pH of the SNSs sols decreased to neutral (pH ~ 7.0) at the final stage of solvent evaporation. For example, the pH of the SNSs sol prepared with *n*-butylamine (initial pH 10.8) drops to pH 6.7 after solvent evaporation by 94.5 wt %. These characteristics should affect the degree of ordering in 3D SNSs arrays. In this section, the structures of assembled SNSs are analyzed by XRD and nitrogen adsorption–desorption. The control of the packing degree of SNSs arrays by the addition of organic additives to the amino acid-free sols is also discussed.

The long-range ordered mesostructures of the assembled SNSs are examined from the information in low-angle by powder XRD. Here, 3D SNSs arrays are formed from the sols prepared with *n*-propylamine, *n*-butylamine, and ammonia by evaporating the solvents at 60 °C. These sols contain monodisperse SNSs with average sizes of 13, 14, and 15 nm, respectively. The XRD patterns of the SNSs arrays after calcination are shown in Figure 5A. Three diffraction peaks that can be indexed as the (111), (220), and (331) reflections of SNSs that are arranged in a face-centered-cubic (fcc) structure²⁵ are observed for all samples. The d_{111} spacings are 11.6, 13.0, and 13.4 nm for SNSs synthesized with *n*-propylamine, *n*-butylamine, and ammonia, respectively. These values are slightly bigger than those expected for close packed structures of SNSs with the sizes of 13, 14, and 15 nm; the ideal d (111) values should be 10.6, 11.4, and 12.2 nm, respectively. These results demonstrate that 3D arrays of SNSs with some degree of ordering can be achieved from SNSs sols prepared with primary amines or ammonia.

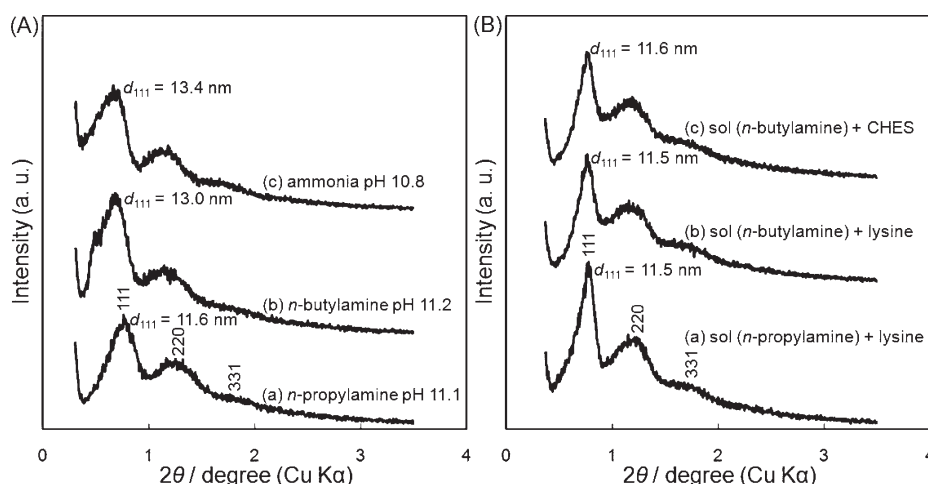


Figure 5. XRD patterns of 3D SNSs arrays obtained by solvent evaporation of (A) SNSs sols that were formed in the presence of different catalysts: (a) *n*-propylamine (pH 11.1), (b) *n*-butylamine (pH 11.2), and (c) ammonia (pH 10.8), and (B) SNSs sols with additives: (a) SNSs sol (*n*-propylamine, pH 11.1) + lysine, (b) SNSs sol (*n*-butylamine, pH 11.2) + lysine, and (c) SNSs sol (*n*-butylamine, pH 11.2) + CHES buffer.

To confirm that the constant pH condition that keeps relatively strong repulsion between SNSs is essential for obtaining 3D well-ordered structure,²⁶ the experiments on the addition of chemical additives with buffering capability to the as-synthesized sols were carried out. Lysine and *N*-cyclohexyl-2-aminoethanesulfonic acid (CHES) were used here as the representative additives. These additives are nonvolatile, thus can maintain the pH of the sol at ~ 9.0 during solvent evaporation. Figure 5B shows the XRD patterns of the SNSs arrays prepared from the corresponding sols containing these additives. The sharper diffraction peaks with slight shifts to the higher angles are observed for all samples, showing that the higher degree of ordering as well as a more ordered close-packed structure is achieved. Both lysine (Figure 5Ba, b) and CHES buffer (Figure 5Bb) are effective for enhancing the degree of ordering.

The 3D arrays of SNSs can be regarded as mesoporous materials. Because the degree of ordering of the SNSs arrays directly affects their pore characteristics, these amino acid-free SNSs can produce mesoporous materials with varying pore sizes and distributions. Nitrogen adsorption analysis gives us information on mesoporous nature of the assembled SNSs. The nitrogen adsorption–desorption isotherm of the 3D arrays of SNSs with the average diameter of 14 nm, prepared with *n*-butylamine at the initial pH of 11.2 followed by solvent evaporation in the absence of any additives (Figure 6Aa), exhibits a capillary condensation step at relative pressure of $P/P_0 = 0.5–0.8$, known as a type IV isotherm according to IUPAC classification.³⁴ Furthermore, the isotherm shows a clear H2 hysteresis loop, which is characterized by a smoothly increasing adsorption branch and a steep desorption branch.³⁵ Commonly, the type H2 hysteresis is attributed to ink bottle shaped pores, having a narrow entrance and a wide inner body. In our case, ink bottle-shaped pores or voids are generated by the arrangement of uniform-sized SNSs.³⁶ The pore size calculated from the adsorption data using the BJH model is ca. 8.1 nm as shown in Figure 6Ba.

Nitrogen adsorption–desorption technique is utilized to further investigate the effects of lysine and buffer on the 3D assembly of SNSs. Interestingly, in the presence of CHES buffer (Figure 6Ab), the hysteresis loop moves to lower P/P_0 , and the pore size shows a relatively narrow distribution centered at 3.9 nm as displayed in Figure 6Bb. It is reasonable to speculate

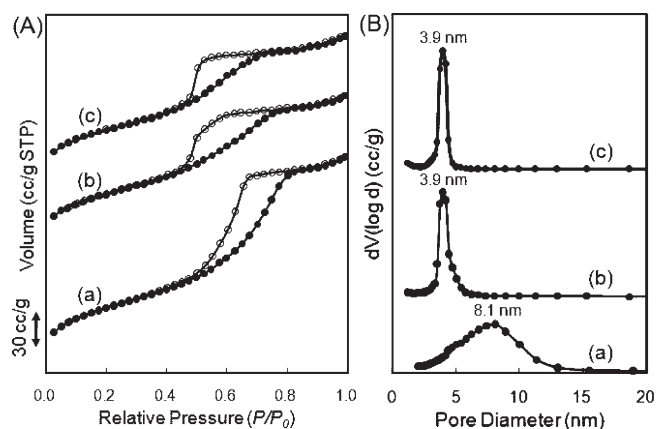


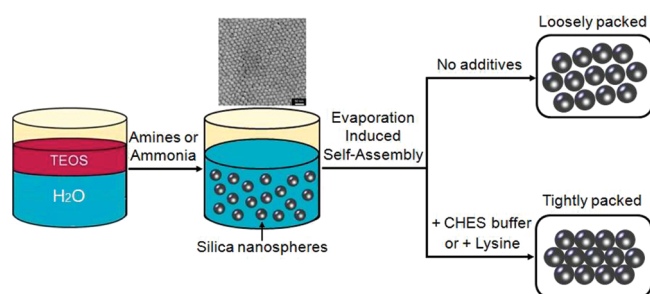
Figure 6. (A) Nitrogen adsorption–desorption isotherms of assembled SNSs obtained by evaporation of silica sols with diameter about 14 nm (pH 11.2, *n*-butylamine catalyst) in the presence of different additives: (a) no additive, (b) CHES buffer, and (c) lysine. Adsorption and desorption points are marked by solid (●) and empty (○) circles, respectively. The isotherms (b) and (c) are offset vertically by 100, and 150 cc g^{-1} , respectively. (B) Corresponding BJH adsorption pore size distribution curves.

that the SNSs assemble into mesostructure more tightly during evaporation process and thereby the smaller mesopore is generated. In the presence of lysine (Figure 6Ac), the hysteresis loop also moves toward lower P/P_0 . Accordingly, Figure 6Bc shows the 3.9 nm uniform mesopore with narrow size distribution, indicating that tightly packed nanostructure is formed. These findings would be consistent with the XRD observations (Figure 5), which pointed to the existence of well-ordered arrangements of SNSs with fcc structure.

The BJH pore size, the total pore volumes, and the packing fraction of the assembled SNSs are summarized in Table 1. With decreasing the mesopore size, the total pore volumes decrease progressively, which is consistent with the formation obtained from the tightly packed nanostructure. To examine the assembled SNSs quantitatively, an important parameter, packing fraction is introduced. For the sake of simplicity, packing fraction is estimated from the total pore volume of the assembled SNSs by

Table 1. Pore Characteristics and Packing Fractions of SNSs Arrays Prepared from Sols That Were Catalyzed by *n*-Butylamine (pH 11.2)

sample name	BJH pore size (nm)	total pore volume (cc/g)	packing fraction (%)
SNSs (no additive)	8.1	0.27	66.1
SNSs + CHES buffer	3.9	0.22	70.5
SNSs + lysine	3.9	0.21	71.5

Scheme 1. Schematic Model Proposed for the Uniform-Sized SNSs Formation and Their Controlled 3D Self-Assembly

assuming the density of silica to be 1.9 g/cm^3 in all calculations.³⁷

$$\begin{aligned} \text{packing fraction} &= 100 - \text{porosity}(\%) \\ &= 100 / (1 + \text{total pore volume} \\ &\quad \times \text{density of silica}) \end{aligned}$$

It is found that packing fraction increases from ca. 66.1% to 70.5–71.5% by adding chemical additives into the as-synthesized SNSs sol prior to evaporation, indicating that the SNSs are packed tightly. The achievable limitation of packing fractions is still smaller than the maximum packing fraction (74%) of the fcc array of ideal hard spheres.

On the basis of the above discussion, the 3D self-assembly process of SNSs is summarized in Scheme 1. SNSs are synthesized in liquid–liquid biphasic system utilizing amines or ammonia as base catalysts. Different packing modes are achieved via solvent evaporation-induced self-assembly. The assembled SNSs with loosely packed nanostructure are formed after direct evaporation of as-synthesized SNSs sol without any additives. In contrast, in the presence of CHES buffer or lysine, SNSs assemble into tightly packed structures.

Without any additives, the decrease in pH to neutral condition (~ 7.0) during evaporation should facilitate the formation of Si–O–Si bonds between the SNSs due to the weakened electrostatic repulsion and increased condensation rate of the surface Si–OH groups, which hinder their rearrangement resulting in a loosely packed nanostructure. In contrast, the pH value is maintained at ~ 9.0 in the presence of CHES buffer or lysine during the whole evaporation period. Owing to the stronger electrostatic repulsion among SNSs and lower condensation rate of Si–OH groups, the SNSs can rearrange freely even at the final stage of evaporation under the influence of capillary force to form tightly packed nanostructure. These results have provided strong evidence that buffer action is extremely important for 3D self-assembly of SNSs into tightly packed structure.

4. CONCLUSIONS

An economical method is demonstrated to synthesize uniform-sized SNSs with diameter in the range of 12–36 nm and size polydispersity below 12% using primary amines or ammonia as base catalysts. The relatively high pH (10.8–11.4) in the liquid–liquid (TEOS–water) biphasic system is the key for synthesizing monodisperse, colloidal SNSs under such unbuffered conditions. The as-synthesized silica sols with near physiological pH exhibit an excellent colloidal stability. Moreover, the SNSs size decreases with the increase in the pH value of the reaction mixture. The chemical additives with buffering capability (e.g., lysine, CHES buffer) play a vital role for preparing well-ordered SNSs arrays. Some significant insights are provided for understanding the 3D self-assembly of small silica nanoparticles. Primary amines or ammonia are the most economical and promising base catalysts for large-scale production with uniform-sized colloidal SNSs. These sols with near physiological pH also hold exciting applications in the biological area (e.g., high-resolution bioimaging).³⁸ In addition, the assembled SNSs arrays provide an ideal hard template for the preparation of various mesoporous materials.³⁹

■ ASSOCIATED CONTENT

S Supporting Information. The pH of the aqueous solutions of base catalysts as a function of their concentrations; SEM images of SNSs synthesized with *n*-butylamine and *n*-propylamine; FT-IR spectra and CHN analysis of SNSs. This material is available free of charge via the Internet at <http://pubs.acs.org>.

■ AUTHOR INFORMATION

Corresponding Author

*Tel: +81-3-5841-7348. Fax: +81-3-5800-3806. E-mail: okubo@chemsys.t.u-tokyo.ac.jp.

■ ACKNOWLEDGMENT

We thank Prof. Yukio Yamaguchi (The University of Tokyo) for zeta potential measurements. We also gratefully acknowledge Dr. Ryotaro Matsuo (Malvern Japan Division of Spectris Co., Ltd.) for nitrogen sorption measurements. J.W. is grateful to Global COE Program “Global Center of Excellence for Mechanical Systems Innovation (GMSI)” of the University of Tokyo, supported by the Ministry of Education, Culture, Sports, Science and Technology (MEXT) of Japan. A.S.-N. acknowledges Grant-in-Aid for Scientific Research on Innovative Areas of “Fusion Materials: Creative Development of Materials and Exploration of Their Function through Molecular Control” (2206) from MEXT.

■ REFERENCES

- (1) Xia, Y. N.; Gates, B.; Yin, Y. D.; Lu, Y. *Adv. Mater.* **2000**, *12*, 693–713.
- (2) Jeong, U.; Wang, Y. L.; Ibisate, M.; Xia, Y. N. *Adv. Funct. Mater.* **2005**, *15*, 1907–1921.
- (3) Park, J.; Joo, J.; Kwon, S. G.; Jang, Y.; Hyeon, T. *Angew. Chem., Int. Ed.* **2007**, *46*, 4630–4660.
- (4) Goesmann, H.; Feldmann, C. *Angew. Chem., Int. Ed.* **2010**, *49*, 1362–1395.
- (5) Iler, R. K. *The Chemistry of Silica: Solubility, Polymerization, Colloid and Surface Properties, and Biochemistry*; Wiley: New York, 1979.

- (6) Brinker, C. J.; Scherer, G. W. *Sol–Gel Science: The Physics and Chemistry of Sol–Gel Processing*; Academic Press: San Diego, 1990.
- (7) Caruso, F. *Adv. Mater.* **2001**, *13*, 11–22.
- (8) Lou, X. W.; Archer, L. A.; Yang, Z. C. *Adv. Mater.* **2008**, *20*, 3987–4019.
- (9) Liu, J.; Liu, F.; Gao, K.; Wu, J. S.; Xue, D. F. *J. Mater. Chem.* **2009**, *19*, 6073–6084.
- (10) Réthoré, G.; Pandit, A. *Small* **2010**, *6*, 488–498.
- (11) Schüth, F. *Angew. Chem., Int. Ed.* **2003**, *42*, 3604–3622.
- (12) Lu, A. H.; Schüth, F. *Adv. Mater.* **2006**, *18*, 1793–1805.
- (13) Liang, C. D.; Li, Z. J.; Dai, S. *Angew. Chem., Int. Ed.* **2008**, *47*, 3696–3717.
- (14) Stein, A.; Li, F.; Denny, N. R. *Chem. Mater.* **2008**, *20*, 649–666.
- (15) Stöber, W.; Fink, A.; Bohn, E. *J. Colloid Interface Sci.* **1968**, *26*, 62–69.
- (16) Giesche, H. *J. Eur. Ceram. Soc.* **1994**, *14*, 205–214.
- (17) Osseo-Asare, K.; Arriagada, F. J. *Colloids Surf.* **1990**, *50*, 321–339.
- (18) Arriagada, F. J.; Osseo-Asare, K. *J. Colloid Interface Sci.* **1999**, *211*, 210–220.
- (19) Chang, C. L.; Fogler, H. S. *Langmuir* **1997**, *13*, 3295–3307.
- (20) Esquena, J.; Tadros, Th. F.; Kostarelos, K.; Solans, C. *Langmuir* **1997**, *13*, 6400–6406.
- (21) Finnie, K. S.; Bartlett, J. R.; Barbé, C. J. A.; Kong, L. *Langmuir* **2007**, *23*, 3017–3024.
- (22) Venditti, F.; Angelico, R.; Palazzo, G.; Colafemmina, G.; Ceglie, A.; Lopez, F. *Langmuir* **2007**, *23*, 10063–10068.
- (23) Jin, Y.; Lohstreter, S.; Pierce, D. T.; Parisien, J.; Wu, M.; Hall, C., III; Zhao, J. X. *Chem. Mater.* **2008**, *20*, 4411–4419.
- (24) Asaro, F.; Benedetti, A.; Freris, I.; Riello, P.; Savko, N. *Langmuir* **2010**, *26*, 12917–12925.
- (25) Yokoi, T.; Sakamoto, Y.; Terasaki, O.; Kubota, Y.; Okubo, T.; Tatsumi, T. *J. Am. Chem. Soc.* **2006**, *128*, 13664–13665.
- (26) Yokoi, T.; Wakabayashi, J.; Otsuka, Y.; Fan, W.; Iwama, M.; Watanabe, R.; Aramaki, K.; Shimojima, A.; Tatsumi, T.; Okubo, T. *Chem. Mater.* **2009**, *21*, 3719–3729.
- (27) Davis, T. M.; Snyder, M. A.; Krohn, J. E.; Tsapatsis, M. *Chem. Mater.* **2006**, *18*, 5814–5816.
- (28) Hartlen, K. D.; Athanasopoulos, A. P. T.; Kitaev, V. *Langmuir* **2008**, *24*, 1714–1720.
- (29) Watanabe, R.; Yokoi, T.; Kobayashi, E.; Otsuka, Y.; Shimojima, A.; Okubo, T.; Tatsumi, T. *J. Colloid Interface Sci.* **2010**, doi: 10.1016/j.jcis.2010.09.001.
- (30) Yokoi, T.; Karouji, T.; Ohta, S.; Kondo, J. N.; Tatsumi, T. *Chem. Mater.* **2010**, *22*, 3900–3908.
- (31) Yamauchi, Y.; Imasu, J.; Kuroda, Y.; Kuroda, K.; Sakka, Y. *J. Mater. Chem.* **2009**, *19*, 1964–1967.
- (32) Snyder, M. A.; Lee, J. A.; Davis, T. M.; Scriven, L. E.; Tsapatsis, M. *Langmuir* **2007**, *23*, 9924–9928.
- (33) Fukao, M.; Sugawara, A.; Shimojima, A.; Fan, W.; Arunagirinathan, M. A.; Tsapatsis, M.; Okubo, T. *J. Am. Chem. Soc.* **2009**, *131*, 16344–16345.
- (34) Sing, K. S. W.; Everett, D. H.; Haul, R. A. W.; Moscou, L.; Pierotti, R. A.; Rouquerol, J.; Siemieniowska, T. *Pure Appl. Chem.* **1985**, *57*, 603–619.
- (35) Morishige, K.; Tateishi, N.; Fukuma, S. *J. Phys. Chem. B* **2003**, *107*, 5177–5181.
- (36) Lee, S.; Cho, I. S.; Lee, J. H.; Kim, D. H.; Kim, D. W.; Kim, J. Y.; Shin, H.; Lee, J. K.; Jung, H. S.; Park, N. G.; Kim, K.; Ko, M. J.; Hong, K. S. *Chem. Mater.* **2010**, *22*, 1958–1965.
- (37) Green, D. L.; Lin, J. S.; Lam, Y.-F.; Hu, M. Z.-C.; Schaefer, D. W.; Harris, M. T. *J. Colloid Interface Sci.* **2003**, *266*, 346–358.
- (38) Atchison, N.; Fan, W.; Brewer, D. D.; Arunagirinathan, M. A.; Hering, B. J.; Kumar, S.; Papas, K. K.; Kokkoli, E.; Tsapatsis, M. *Angew. Chem., Int. Ed.* **2011**, *50*, 1617–1621.
- (39) Lee, P. S.; Zhang, X. Y.; Stoeger, J. A.; Malek, A.; Fan, W.; Kumar, S.; Yoo, W. C.; Hashimi, S. A.; Penn, R. L.; Stein, A.; Tsapatsis, M. *J. Am. Chem. Soc.* **2011**, *133*, 493–502.